Supporting information

Used Tissue Paper as a 3D Substrate for Non-enzyme Glucose Sensors

Zhiyu Chen[a], Lei Li[a], Xuanyu Xiao[a], Yuxin Zhang[a], Jieyu Zhang[a], Qing Jiang[a,*], Xuefeng Hu[b,*], Yunbing Wang[a,*]

[a] National Engineering Research Center for Biomaterials & College of Biomedical Engineering, Sichuan University, Chengdu, Sichuan, 610065, China

[b] West China School of Basic Medical Sciences & Forensic Medicine, Sichuan University, Chengdu, Sichuan

* Corresponding author. 29 Wangjiang Road, Chengdu, China, 610065

Tel: +86 028 85410537; Fax: +86 028 85410246

E-mail addresses: jiangq@scu.edu.cn (Q. Jiang), huxuefeng@scu.edu.cn (X. Hu), yunbing.wang@scu.edu.cn (Y.Wang)

1. Method

1.1 Calcination

The Au-Pt-PANs were placed in a crucible after they were completely dried (the crucible is washed with ethanol in advance to avoid the influence of impurities). Then, Au-Pt-PANs were heated to 600 °C at a heating rate of 5 °C min^{-1} with a gas flow of N_2 (20 sccm) in a quartz tube of the tube furnace. Hereafter, the temperature was maintained for 3h. After that, the resultant was naturally cooled to room temperature under the N_2 atmosphere(about 3h) and then the PAAPNs were obtained.

1.2 Characterization

Morphologies and structure characteristics were studied by using a scanning electron microscope (SEM, Thermo Helios G4 UC) equipped with an energy-dispersive X-ray (EDX) 6 detector for elemental analysis. The transmission electron microscope (TEM) and high-resolution TEM (HRTEM) images and selected area electron diffraction (SAED) patterns were acquired using a Talos F200X S/TEM with a field-mission gun operating at 200 kV. X-ray diffraction (XRD) tests were performed by a Rigaku Ultima IV instrument with Cu Kα (target) radiation (λ = 1.5418 Å) with a scanning rate of 2 °/min in the 2θ range of 5 ° to 90 °. Raman analysis was performed using a Raman spectrometer (Thermo Dxr2xi) employing a laser with a 785 nm excitation wavelength as the excitation source. X-ray photoelectron spectroscopy (XPS) was carried out on a Thermo Escalab 250Xi system by using an XPS spectrometer with a dual Al Ka X-ray source. Deconvolution of overlapping peaks was performed by a mixed Gaussian-Lorentzian fitting program (Thermo Avantage).

1.3 Anti-interfering test

For the anti-interference tests of Figure 2h, 1 mM concentration of glucose and 0.1 mM concentrations of interferents were successively added to the electrolyte (0.01 M PBS) in the three-electrode system at the different applied potentials of -0.2 to 0.2 V. Ran the workstation for 1h under the electrolyte before each different applied potential test to ensure a stable baseline. The

difference between the current data at 600s and the baseline was recorded as the response current of the test object.

1.4 Cellular viability

L929 fibroblast cells (American Type Culture Collection, USA) were incubated in HyClone™ Dulbecco's Modified Eagles Medium (DMEM) (GE Life Sciences, China) containing 10 % fetal bovine serum (FBS) and 1 % penicillin-streptomycin at 37 ℃ in a 5 % CO_2 atmosphere. The cells were seeded in a 96-well plate (2×103 cells/well) for 24 h. For the direct contact method, the silicon wafers (1 cm × 1 cm × 1 mm) loaded with equal concentrations of PAAPNs or PAAPNs/Nafion were gently placed on top of the cells. The silicon wafers were removed, and the MTT assay was used to determine cell viability. For the extract method, the silicon wafers were incubated in 15 mL DMEM at 37 ℃ for 24 h to prepare the extract. The seeded cells in the 96-well plate were cultured in the extract for 24 h, and the cellular viability was tested by MTT assay.

1.5 Density functional theory (DFT) calculation

All the calculations were performed in the framework of DFT as implemented with the Dmol3 module of Materials Studio 2017 R2[1]. The exchange-correlation potential was described using the generalized gradient approximation (GGA) added in the form of the Perdew-Burke-Ernzerhoff (PBE) functional[2,3]. The dual numerical polarization (DND 4.4) all-electron basis set was selected as the electronic basis set. A 5 × 5 unit cell of graphene with a slab separated by a vacuum region of 30 Å was built as an adsorption substrate. Brillouin zone integration was performed on a 4 × 4 × 1 Monkhorst-Pack grid [4]. A Fermi smearing of 0.01 Ha and a global orbital cutoff of 4.5 Å were employed. The convergence of the self-consistent iterations was settled for the charge density variation within 1×10^{-6}. All the structures were relaxed until the residual forces on each atom had declined to less than 0.002 Ha/Å. First, a 5 × 5 single-layer graphene was constructed and optimized. The relaxed lattice constraints were 12.336 Å ×12.336 Å. Afterward, single Au, Pt atoms and Pt-doped Au clusters were adsorbed on the graphene substrate, followed by structure optimization. Then, a glucose monomer was bonded to the Au or Pt atom. The whole system was relaxed again. After obtaining stable configurations, the density of states for considered systems was computed. After the glucose adsorption, the charge density difference ($\Delta\rho$) was calculated

using the CASTEP module as follows: $\Delta\rho = \rho_{total} - \rho_{GNS\text{-}metal} - \rho_{glucose}$, Where ρ_{total}, $\rho_{GNS\text{-}metal}$, and $\rho_{glucose}$ were the total charge density of the GNS-catalyst-glucose system, the GNSs-catalyst system, and the glucose monomer, respectively.

Table S1 Carbon-based enzymatic sensors and Pt-based nonenzymatic sensors performance taken from literature

Materials	Method	Detection limit (mmol L^{-1})	Detection range (mmol L^{-1})	Sensitivity (μA mM^{-1} cm^{-2})	Ref.
Oil-based Pt@CNOs	Burning to collect ash + calcination + high-temperature reflux + chemical deposition + high-temperature reflux	0.21	2-28	21.6 (under +0.45 V)	5
Lignin-polylactic acid-based CNF/Gox	Electrospinning + thermal oxidation stabilization + calcination + nitric acid etching + enzyme immobilization	0.089	0.15-2.7	50 (under -0.56 V)	6
Au@Pt nanoparticles	Chemical deposition + centrifugation + electrodeposition	0.0004	0.01-10	0.0986/cm^2 (unknown area) (under +0.35 V)	7
Filter paper-based GOx/Fc-COOH	Two steps of physical deposition	0.18	1-5	0.32 (under +0.25 V)	8
Reduced graphene/ cellulose matrix Pt nanoparticles	Stirring and centrifuging several times + in situ solvothermal reduction method	0.002 (in NaOH electrolyte)	0.005-8 (in NaOH electrolyte)	76.9 (in NaOH electrolyte) (under +0.1 V)	9
Graphene oxide-functionalized graphene/ GOx/ Chitosan	Physical deposition + electrodeposition	0.08	0.1-3	46.71 (under -0.5 V)	10
Au/Au-Pt nanoparticles carbon paper fiber	Chemical deposition + calcination	0.21	0.25-36	0.29 (under -0.1 V)	This work

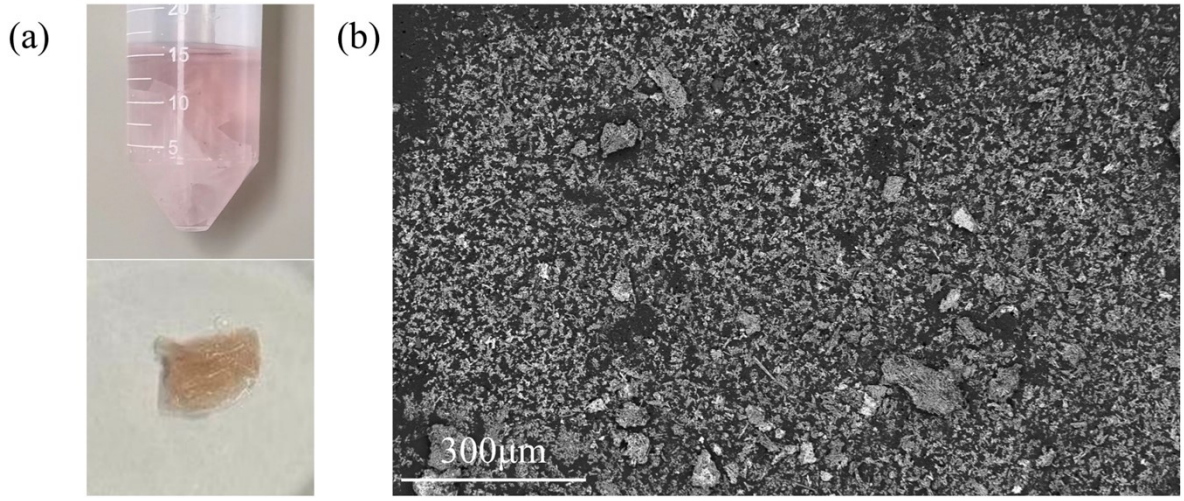

Figure S1. (a) Image of the tissue paper for recycling in the 90 mM NaOH solution. Au NPs were deposited on the paper indicated by the purple-red color. (b) SEM image of PAAPNs on the GCE after the test (300 μm).

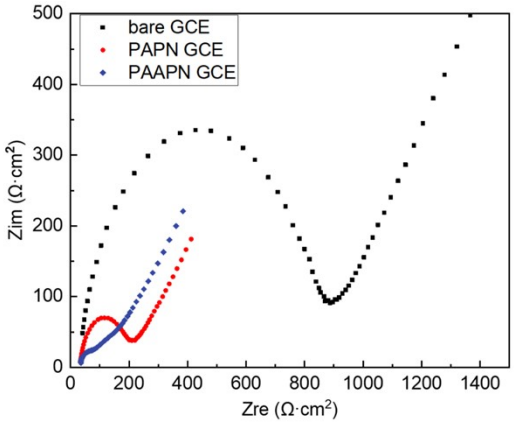

Figure S2. EIS test result of the bare GCE, PAPN (PAAPNs without initial deposition of Au nanoparticles), and PAAPNs electrodes.

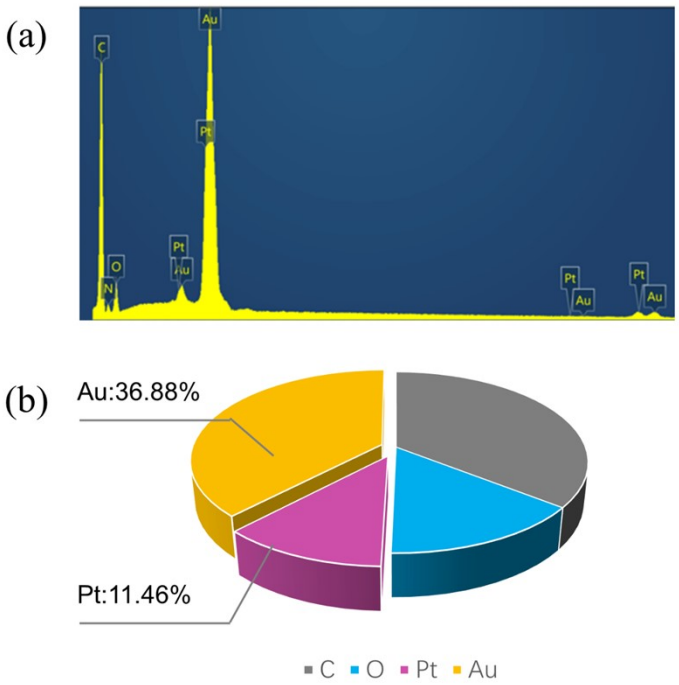

Figure S3. Result of EDS analysis. (a) the intensity peaks of main elements. (b) the pie chart of weight% for the main elements.

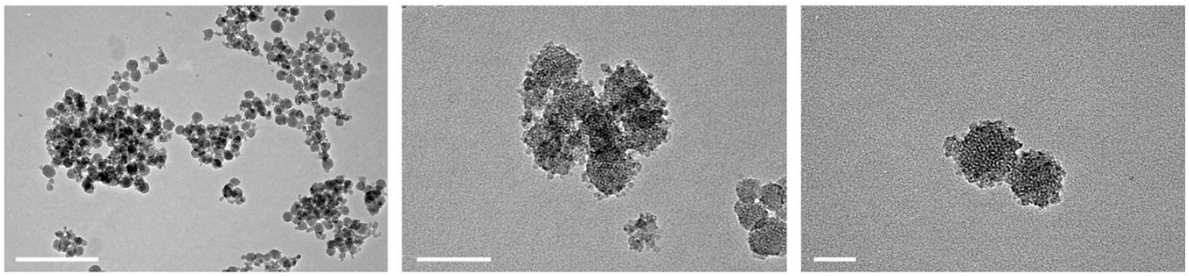

Figure S4. TEM images of Au-Pt nanoparticles (500 nm, 100 nm, and 50 nm, respectively). Both Au and Pt nanoparticles are tightly wrapped on the surface of the Brij 58®, and the size of the particles is ~60 nm.

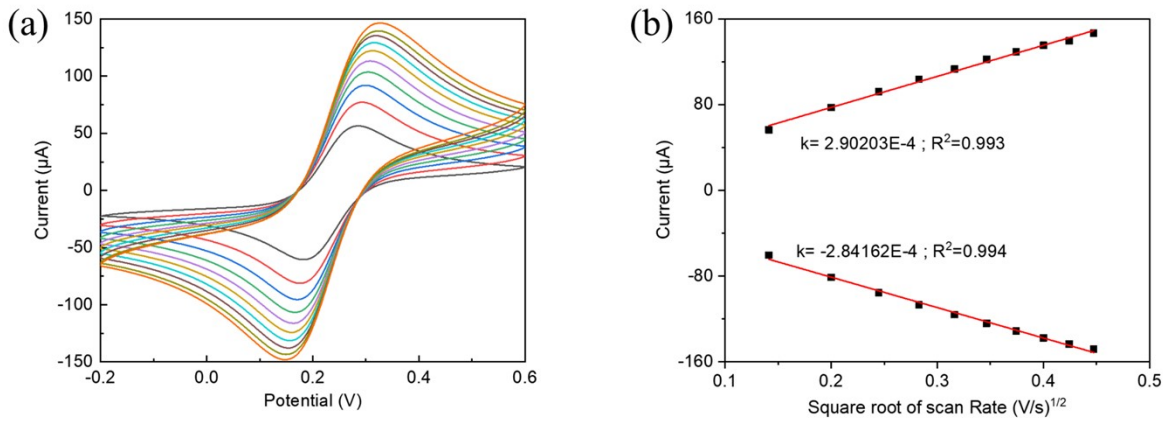

Figure S5. (a) CVs of the PAAPNs in $Fe(CN)_6^{3-/4-}$ at different scan rates from 20 to 200 mV/s (without glucose). (b) The linear relationship of the current density with the scan rate of the PAAPNs.

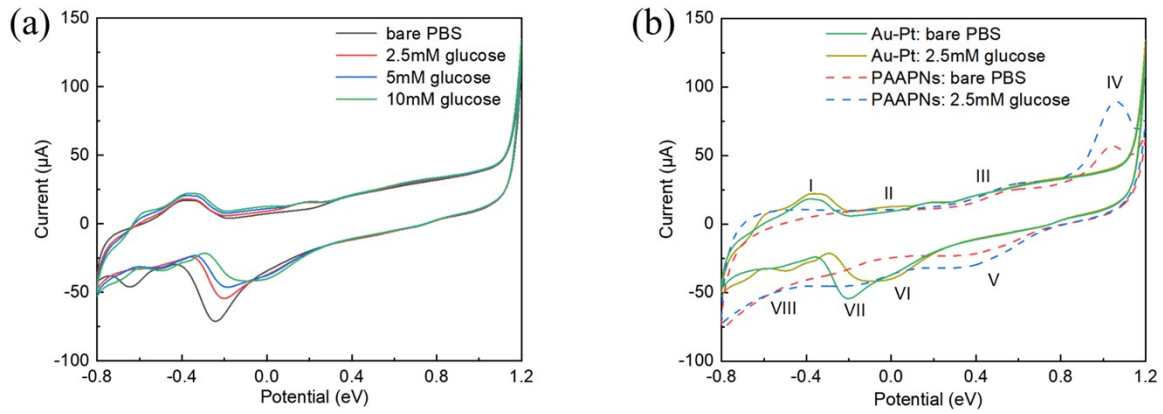

Figure S6. (a) CV curves of the Au-Pt electrode in 0.01 M PBS at the scan rate of 100 mV/s at various glucose concentrations (0-10 mM). (b) The CV curves for the comparison between the Au-Pt and PAAPNs electrodes in the electrolyte of 0.01 M PBS and 2.5 mM glucose (both were tested after multiple cycles of scanning).

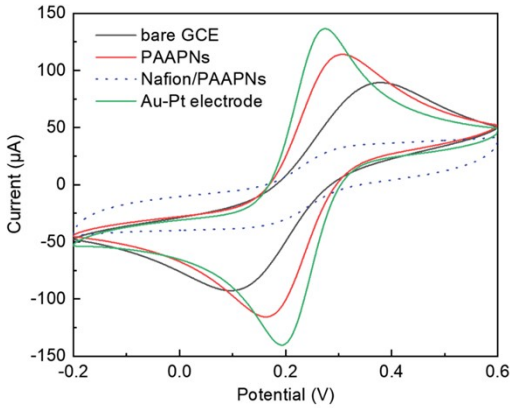

Figure S7. CV curves of bare GCE, PAAPNs, Nafion/PAAPNs and Au-Pt electrodes in $Fe(CN)_6^{3-/4-}$ (without glucose).

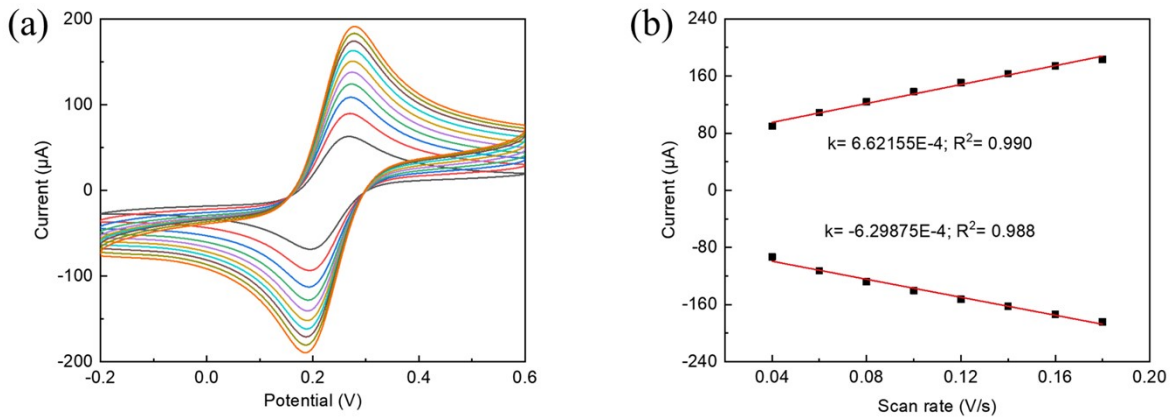

Figure S8. (a) CVs of the Au-Pt electrodes in $Fe(CN)_6^{3-/4-}$ at different scan rates from 20 to 200 mV/s (without glucose). (b) The linear relationship of the current density with the scan rate of the Au-Pt electrodes.

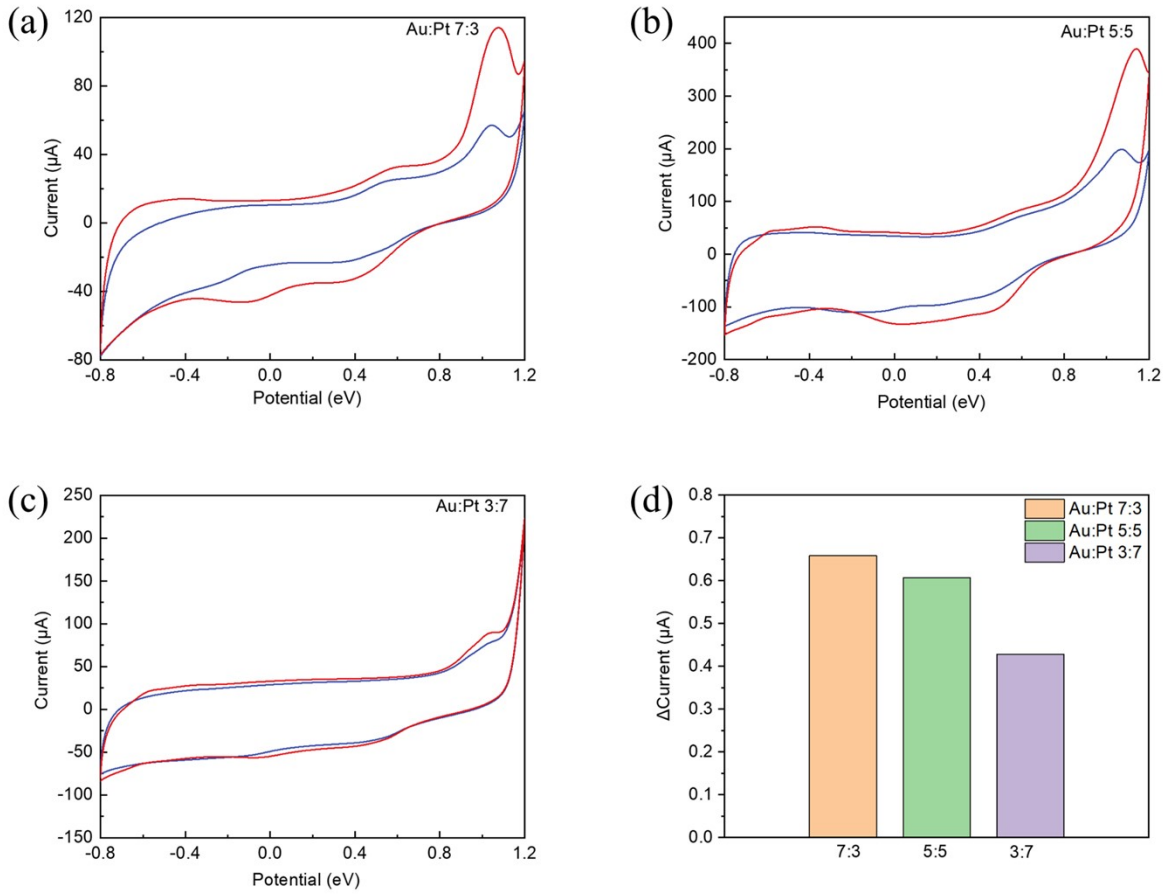

Figure S9. (a-c) CVs of the PAAPNs electrodes fabricated using different precursor deposition solution ratios. (a) 7:3 $HAuCl_4$/ H_2PtCl_6 ratio. (b) 5:5 $HAuCl_4$/ H_2PtCl_6 ratio. (c) 3:7 $HAuCl_4$/ H_2PtCl_6 ratio. (d) Oxidation current at the potential of -0.1 V in the CVs of 5 mM glucose for different H_2PtCl_6/$HAuCl_4$ ratios.

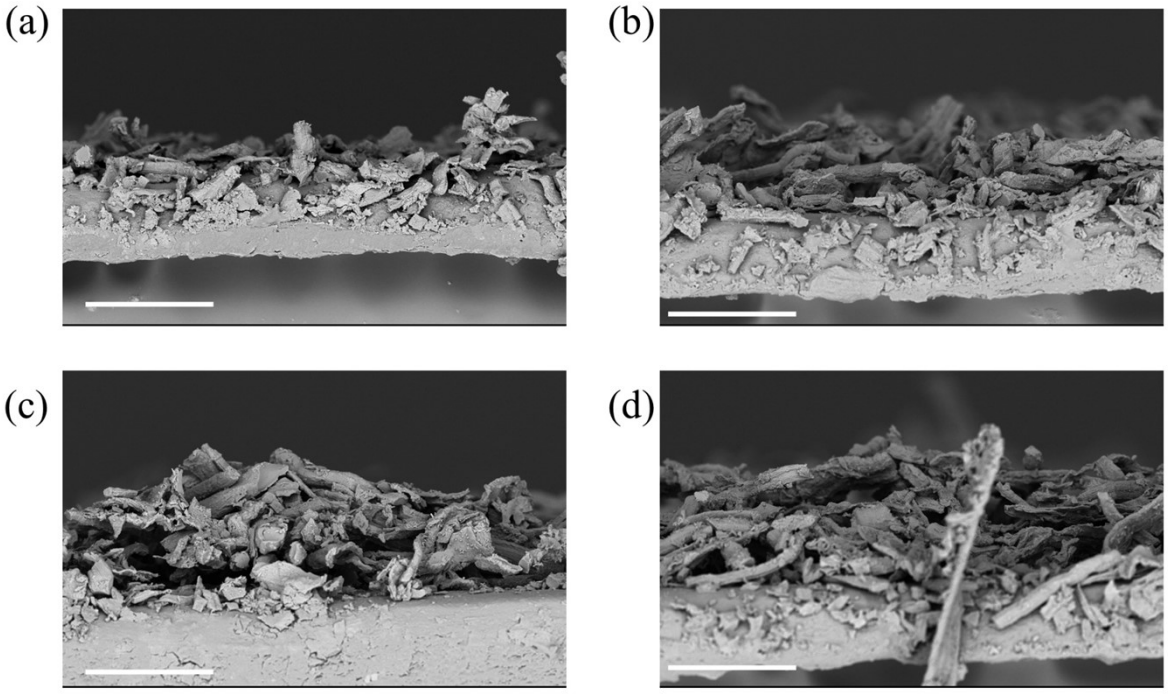

Figure S10. SEM of paper-printed electrode cross-section for 3 μL(a), 5 μL(b), 7 μL(c), 10 μL(d) PAAPNs suspension droplet loading (50 μm).

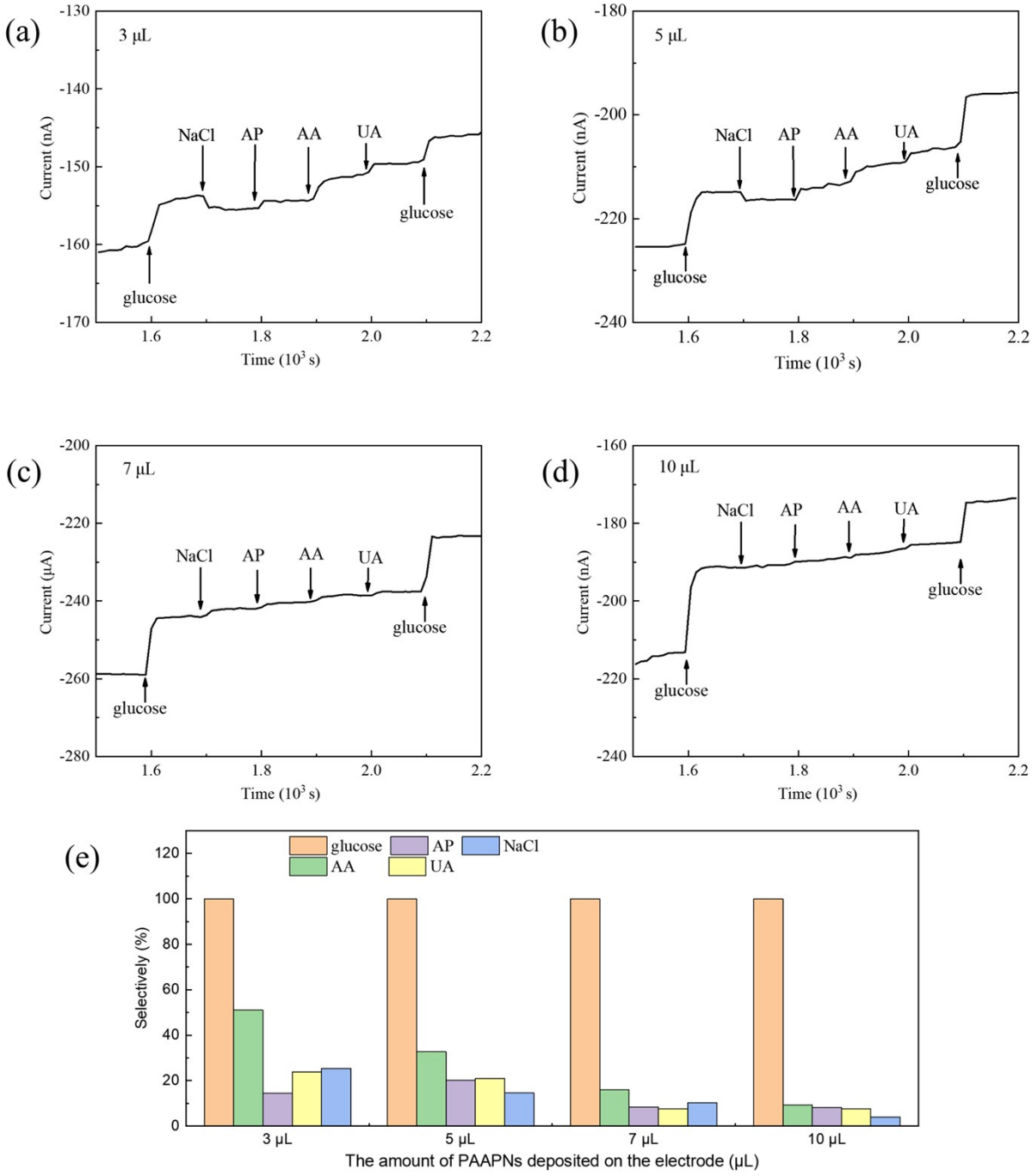

Figure S11. Amperometric (i–t) curve at -0.1 V for the anti-interference test of 3 μL(a), 5 μL(b), 7 μL(c), and 10 μL(d) drop volume respectively. (e) Effect of drop volume on the selectivity of the PAAPNs.

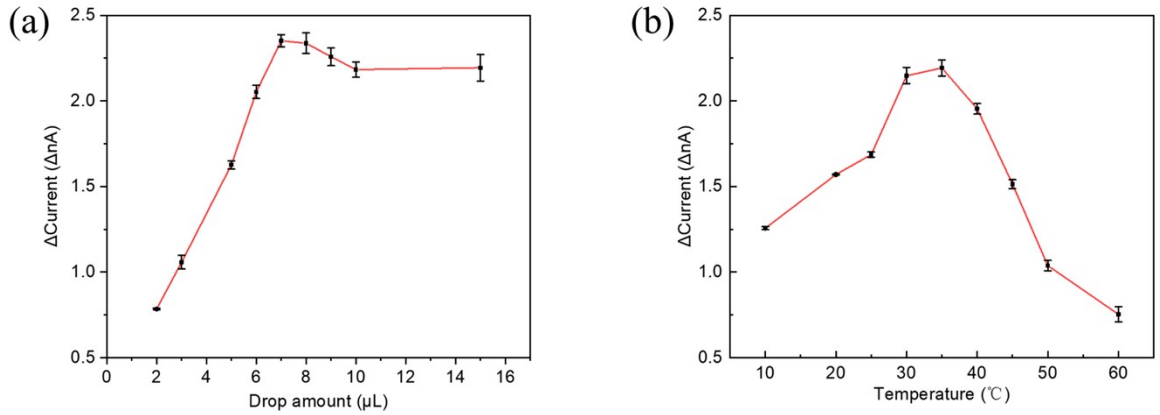

Figure S12. Optimization of the experimental parameters: (a) the effects of the amount of PAAPNs dispersions. (b) temperature on the response current in 0.01 M PBS (pH 7.4) containing 0.1 mM glucose.

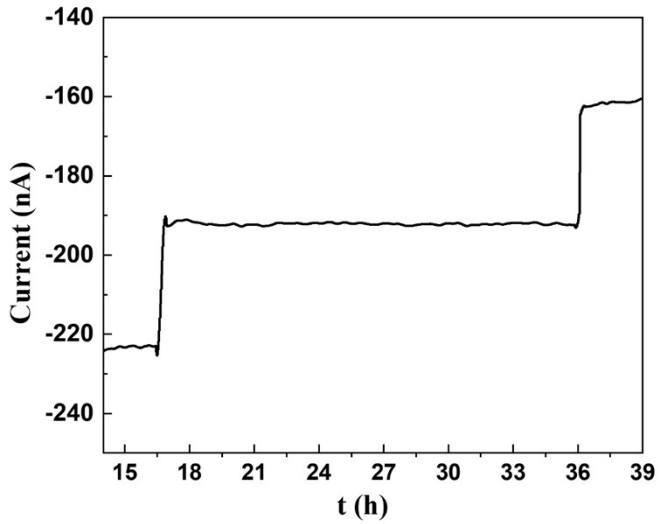

Figure S13. PAAPNs sensor stability testing. With the addition of a 10 mM concentration of glucose at about 16 h, the current was basically stable for about 20 h, then proceed to add 10 mM glucose. During these 20 hours, the maximum change in current does not exceed 5% of the current response, and the sensitivity remained almost the same after adding another 10 mM glucose.

Figure S14. The data record on the SMBG after the test.

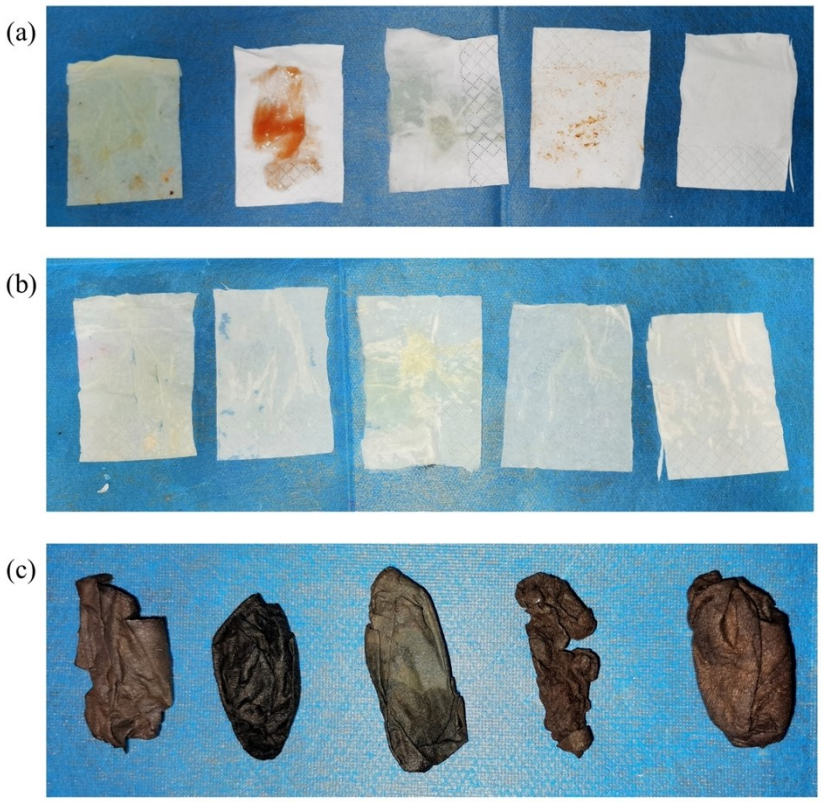

Figure S15. (a) Kitchen waste tissue dipped separately in orange juice, tomato sauce, vegetable oil, chili powder, or tap water (from left to right). (b) Different kitchen waste tissue soaked in ethanol for 1 day. (c) Different kitchen waste tissue-based PAAPNs after calcination. (the order of (b) and (c) remain the same as (a))

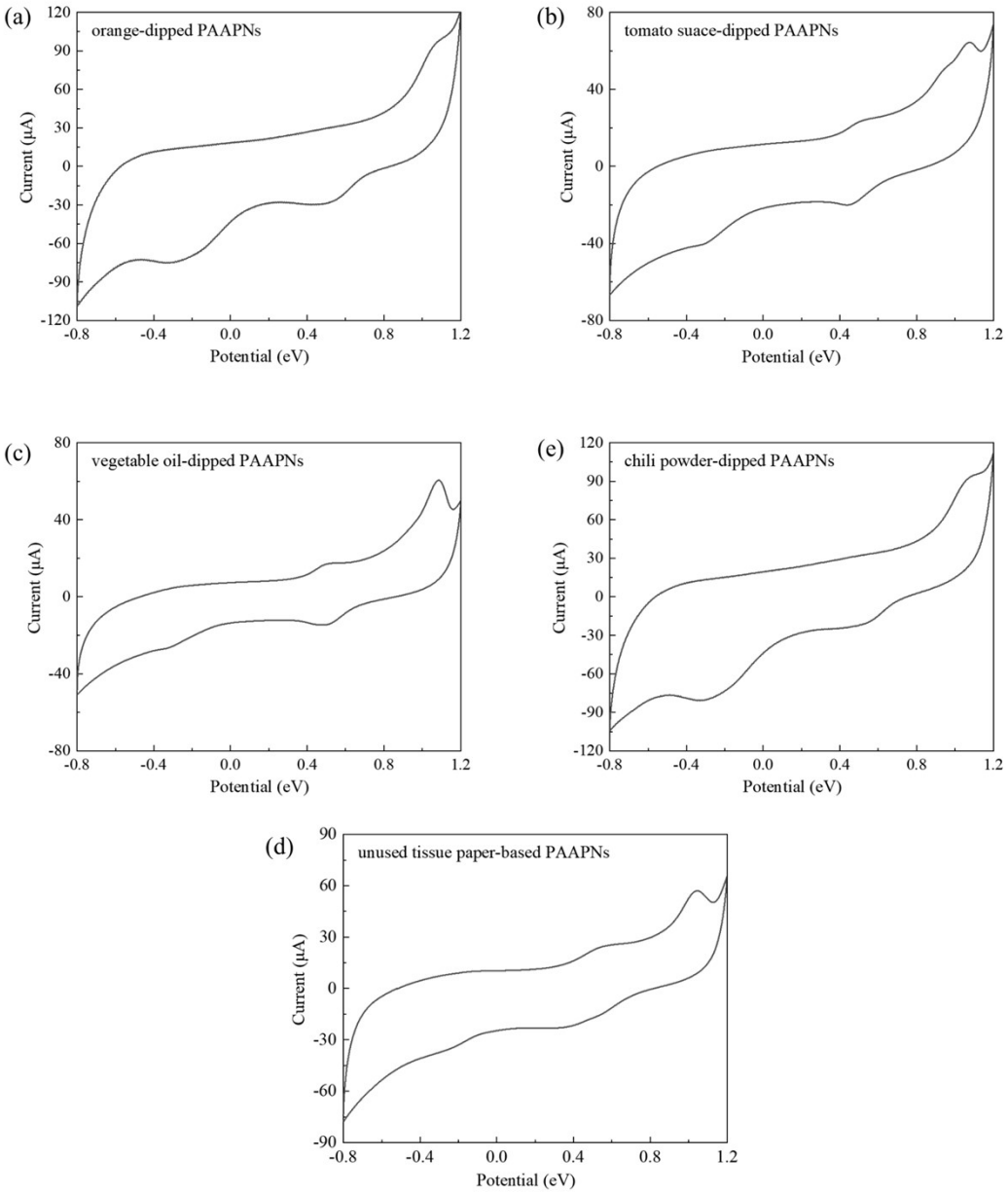

Figure S16 CVs of different types of kitchen waste tissue based on Figure S1. All the CVs show the same oxidation and reduction peaks, the slight difference in CVs is due to the construction of tissue carbon fiber.

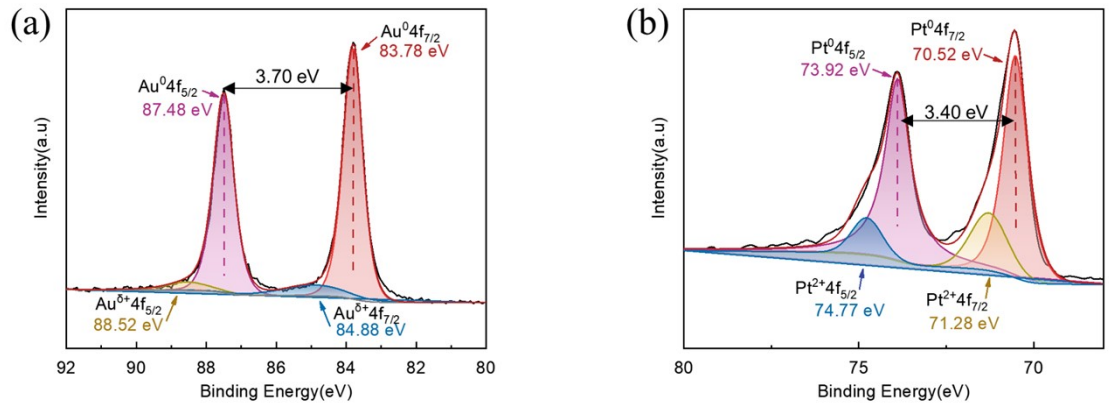

Figure S17. XPS core-level spectra of Au and Pt wires. (a) Au 4f. (b) Pt 4f.

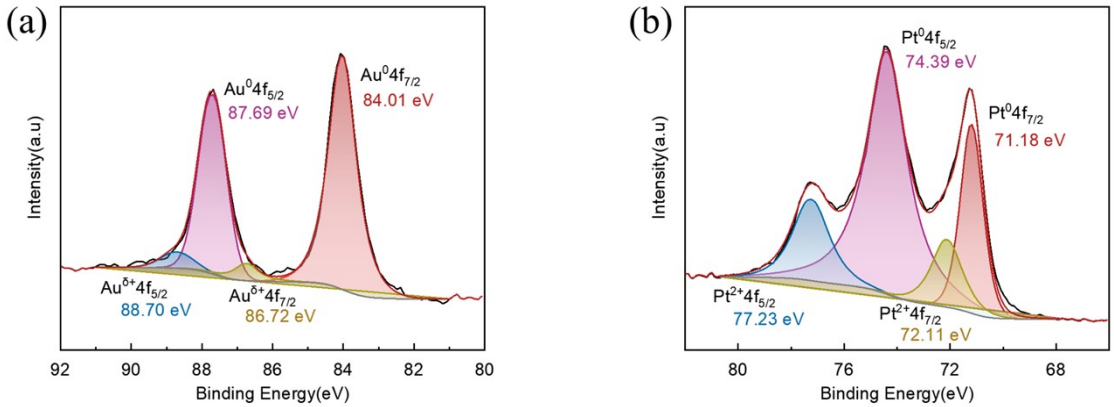

Figure S18. XPS core-level spectra in Au_3Pt_7. (a) Au 4f. (b) Pt 4f.

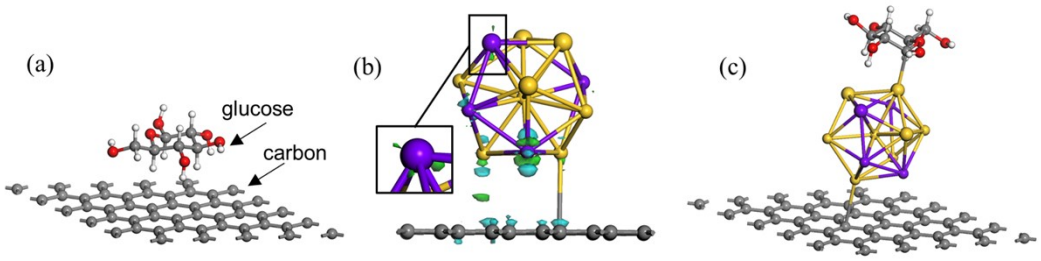

Figure S19. (a) Geometrically optimized structure of the graphene-glucose composite. (b) 3D charge density of the Au-Pt-graphene structure. (c) Glucopyranose adsorption on the Au-Pt-graphene, but suppose. Cyan and green iso-surface represent charge accumulation and depletion in the 3D space with an iso-surface value of 0.005 e A^{-3}. Yellow, purple, grey, red, and white balls represent Au, Pt, C, O, and H atoms.

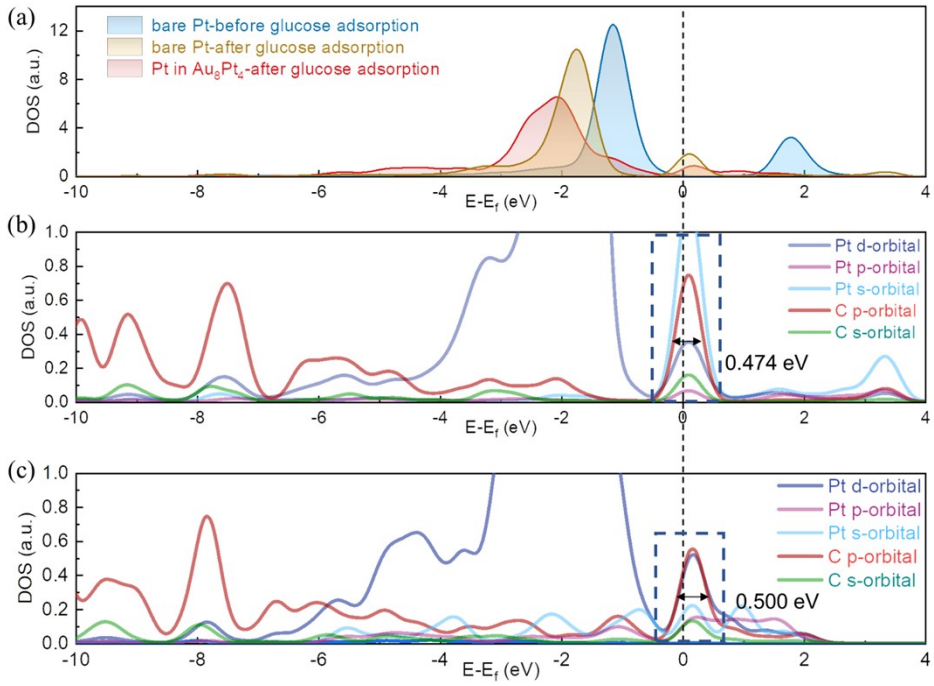

Figure S20. (a) Total DOSs of the bare Pt and Pt in Au_8Pt_4 before and after glucose adsorption. (b) Partial DOS spectra of bare Pt after glucose adsorption and the spectra of C in glucose adsorbed on bare Pt. (c) Partial DOS spectra of Pt in Au_8Pt_4 after glucose adsorption and the spectra of C in glucose adsorbed on Pt.

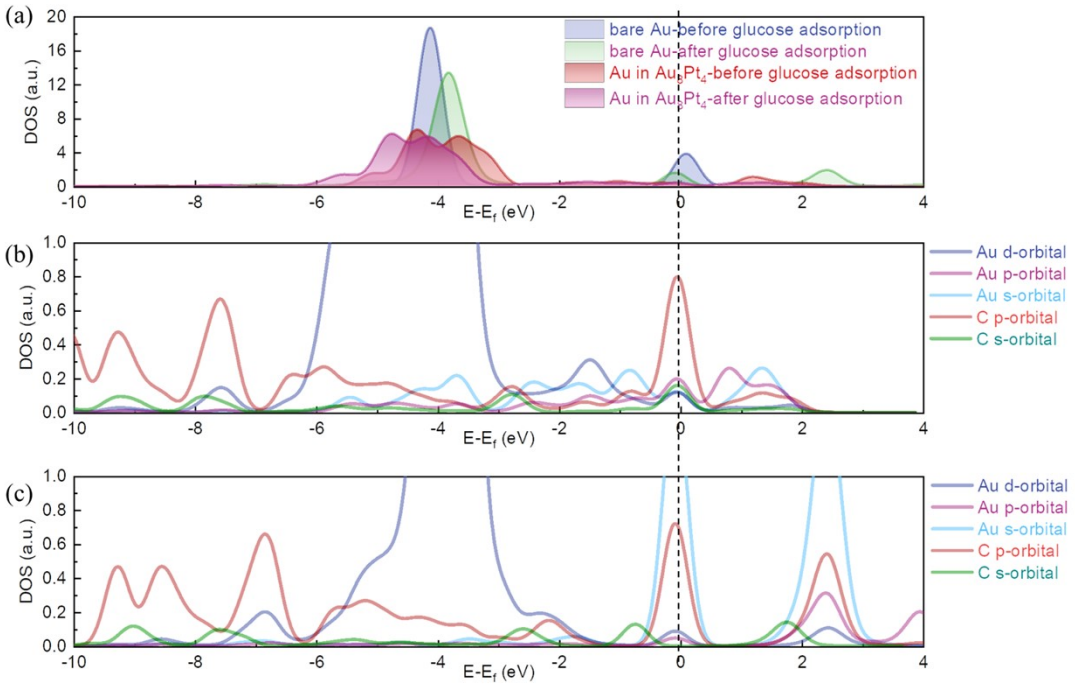

Figure S21. (a) Total DOSs of bare Au and Au in Au_8Pt_4 before and after the glucose adsorption. (b) Partial DOS spectra of Au in Au_8Pt_4 after glucose adsorption and the spectra of C in glucose adsorbed on Au. (c) Partial DOS spectra of bare Au after glucose adsorption and the spectra of C in glucose adsorbed on bare Au.

Reference

1. B. Delley, *J. Chem. Phys.*, 2000, **113**, 7756-7764, Pii [s0021-9606(00)30342-7].
2. J. P. Perdew, K. Burke and Y. Wang, *Phys. Rev. B.*, 1996, **54**, 16533-16539.
3. J. P. Perdew, K. Burke and M. Ernzerhof, *Phys. Rev. Lett.*, 1996, **77**, 3865-3868.
4. H. J. Monkhorst and J. D. Pack, *Phys. Rev. B.*, 1976, **13**, 5188-5192.
5. J. Mohapatra, B. Ananthoju, V. Nair, A. Mitra, D. Bahadur, N. V. Medhekar and M. Aslam, *Appl. Surf. Sci.*, 2018, **442**, 332-341.
6. A. Beaucamp, M. Culebras and M. N. Collins, *Green Chem.*, 2021, **23**, 5696-5705.
7. K. Shim, W. C. Lee, M. S. Park, M. Shahabuddin, Y. Yamauchi, M. S. A. Hossain, Y. B. Shim and J. H. Kim, *Sensor Actuat. B-Chem.*, 2019, **278**, 88-96.
8. C. S. K. Lawrence, S. N. Tan and C. Z. Floresca, *Sensor Actuat. B-Chem.*, 2014, **193**, 536-541.
9. L. Dong, S. Ren, X. Zhang, Y. Yang, Q. Wu and T. Lei, *Carbohyd. Polym.*, 2023, **303**, 120463.
10. Y. Hao, M. Fang, C. Xu, Z. Ying, H. Wang, R. Zhang, H.-M. Cheng and Y. Zeng, *Journal of Materials Science & Technology*, 2021, **66**, 57-63.